



CrossMark
click for updates

Cite this: *RSC Adv.*, 2014, 4, 49295

Environmentally benign enhanced hydrogen production *via* lethal H₂S under natural sunlight using hierarchical nanostructured bismuth sulfide†

U. V. Kawade, R. P. Panmand, Y. A. Sethi, M. V. Kulkarni, S. K. Apte, S. D. Naik and B. B. Kale*

Nanorods and hierarchical nanostructures (dandelion flowers) of bismuth sulfide (Bi₂S₃) were synthesized using a solvothermal method. The effects of solvents such as water and ethylene glycol on the morphology and size of the Bi₂S₃ nanostructures were studied. A structural study showed an orthorhombic phase of Bi₂S₃. We observed nanorods 30–50 nm in diameter and dandelion flowers assembled with these nanorods. A formation mechanism for the hierarchical nanostructures of Bi₂S₃ is proposed. Based on the tuneable band gap of these nanostructures in the visible and near-IR regions, we demonstrated the photocatalytic production of hydrogen from H₂S under normal sunlight. Abundantly available toxic H₂S was used to produce hydrogen under normal sunlight conditions. We observed an excellent hydrogen production of 8.88 mmol g⁻¹ h⁻¹ under sunlight (on a sunny day between 11.30 am and 2.30 pm) for the Bi₂S₃ flowers and 7.08 mmol g⁻¹ h⁻¹ for the nanorods. The hierarchical nanostructures suppress charge carrier recombination as a result of defects, which is ultimately responsible for the higher activity. The evolution of the hydrogen obtained is fairly stable when the catalyst is used repeatedly. The evolution of hydrogen *via* water splitting was observed to be lower than that *via* H₂S splitting. Bi₂S₃ was observed to be a good eco-friendly photocatalyst active under natural sunlight. The photo-response study showed that the Bi₂S₃ microstructures are good candidates for applications in highly sensitive photo-detectors and photo-electronic switches.

Received 15th July 2014
Accepted 5th September 2014

DOI: 10.1039/c4ra07143c

www.rsc.org/advances

1. Introduction

Hydrogen is an important clean energy source and investigations have been carried out worldwide to find new methods of producing hydrogen at cheaper cost. In 1972, Fujishima and Honda¹ reported the solar light-assisted splitting of water using TiO₂, which opened new doors in the field of solar energy conversion. This photocatalytic process has attracted much attention and appears to be a promising strategy for clean, low-cost and environmentally safe hydrogen production using solar energy.^{2–4a} The photo-cleavage of H₂S to H₂ and S is of immense importance because of the need to dispose of H₂S and the environmental problems associated with this disposal. Acidic H₂S is a product of oil refineries and is both toxic and corrosive in nature, creating a number of environmental problems. The currently used Claus process has limitations and uses only negligible amounts of H₂S in the preparation of liquid sulphur for use in agriculture and the pharmaceutical industry. The

photo-splitting of H₂S for the production of hydrogen and sulphur is of interest because this reaction requires less energy (79.9 kJ mol⁻¹) than the photo-splitting of water (285.83 kJ mol⁻¹). Bismuth sulfide (Bi₂S₃) is known to be effective in the splitting of water. There have been a number of reports on the splitting of water using Bi₂S₃ as a photocatalyst.^{4b} We have demonstrated the photocatalytic production of H₂ from H₂S using a variety of nanostructured photocatalysts.^{5–10e} However, from the commercial point of view, there is a need for a highly efficient and stable catalyst. In this context, a nanostructured Bi₂S₃ photocatalyst has been studied for hydrogen production from H₂S.

Bi₂S₃ is a semiconductor material with a direct band gap of 1.3 eV (ref. 11–13) and has numerous potential applications in photovoltaics, IR spectrometry and thermoelectric devices. It is also used in the synthesis of zeolites and other inorganic materials, as an imaging agent in X-ray computed tomography, and as a liquid junction solar cell. In photocatalysis, Bi₂S₃ in composite form has been used as a photocatalyst for the degradation of organic dyes.^{14,15} Composites such as Bi₂S₃/TiO₂ and Bi₂O₃/Bi₂S₃ have also been reported for use in the photo-electrochemical evolution of hydrogen, as well as the photochemical production of hydrogen from water.^{16–19} A photoelectrochemical water splitting and photo-response study has also been reported.¹⁶

Centre for Materials for Electronics Technology (C-MET), Department of Electronics and Information Technology (DeitY), Government of India, Panchwati, Pune-411 008, India. E-mail: bbkale@cmet.gov.in; kbbb1@yahoo.com

† Electronic supplementary information (ESI) available. See DOI: 10.1039/c4ra07143c

As a result of the encouraging properties of hierarchical nanostructures, research has recently been focused on the fabrication of controlled size and shaped hierarchically assembled nanostructures. Many researchers have studied various morphologies, such as nanotubes, nanoparticles,²⁰ nanowires,^{21,22} nanorod bundles and dandelion-like nanostructures,²³ and urchin-like nanospheres²⁴ using various methods of synthesis. However, the use of nanostructured Bi₂S₃ as a photocatalyst for the generation of hydrogen from the splitting of H₂S under visible light has not been studied in detail. More significantly, the effect of Bi₂S₃ nanostructures on its photocatalytic activity in sunlight has not been thoroughly investigated. In view of this, we synthesized Bi₂S₃ nanostructures (nanorods/hierarchical nanostructures) and studied their photocatalytic activity.

Herein, the photo-cleavage of waste H₂S to H₂ under normal sunlight using a Bi₂S₃ semiconductor photocatalyst is reported. The effect of Bi₂S₃ nanostructures, such as nanorods and hierarchical nanostructures on the production of hydrogen and its mechanism of action has been investigated. The evolution of hydrogen *via* water splitting was also investigated using these nanostructures. The structural and optical study of these nanostructures have also been reported.

2. Experimental

2.1. Material synthesis

All the reactants and solvents were of analytical-reagent grade and purchased from a reputable firm. The Bi₂S₃ nanostructures were prepared by dissolving 2 mmol of Bi(NO₃)₃·5H₂O and 8 mmol of thiourea (TU) in 80 mL of aqueous solvent [1 : 3 water-ethylene glycol (EG)]. After stirring for 1 h, the solution was transferred into a 100 mL Teflon-lined stainless-steel autoclave. The system was then sealed and placed in an oven at 150 °C. After reaction, the system was naturally cooled to room temperature and the black precipitate obtained was filtered and washed several times with water and ethanol. The product was dried at 80 °C and used for further characterization. Sample S1 was synthesized in water with a reaction time of 24 h. Samples S2 and S3 were synthesized in water-EG (1 : 3) with reaction times of 24 and 30 h, respectively.

2.2. Characterization

The structural investigation was carried out using an X-ray diffractometer (Model-D8, Advance and Bruker AXS). The morphology was observed by FESEM (JEOL, IIT Roorkee and Hitachi S-4800). The morphology and crystal size were also confirmed by transmission electron microscopy (FEI-Technai). The optical study was performed using a UV-visible spectrometer (Model-Lambda-950, PerkinElmer). The photoluminescence of the synthesized material was recorded on a Horiba Fluorolog 3 spectrofluorometer. The single-point BET surface area was measured using a Quantachrome instrument. The variation in current was measured using an electrometer workstation (Keithley Electrometer, 6517B) with light illumination.

2.3. Photo-responsive properties

The experimental setup for the measurements of the photo-responsive properties of the Bi₂S₃ nanostructures is given in the ESI.† A photo-responsive device was built using the as-synthesized Bi₂S₃ hierarchical microstructures following the device configuration shown in Fig. SI 1.† The ITO substrate with an area of 1 × 2 cm² was etched by dilute HF in an area of dimensions 0.2 × 1 cm² and the ITO film was then divided in two parts, which acted as dual electrodes (see Fig. SI 1.†). A white-light LED lamp (8 mW m⁻²) was used as the illumination source and a bias voltage (typically 20 mV) was applied on the ITO electrode.

2.4. Photocatalytic study for H₂S splitting

The cylindrical quartz photochemical thermostatic reactor was filled with 700 mL of 0.5 M aqueous KOH and purged with Ar for 1 h. H₂S was bubbled through the solution at a rate of 2.5 mL min⁻¹ at 298 K. H₂S was continuously fed into the system during the photo-reduction. Bi₂S₃ was introduced into the reactor and irradiated with normal solar light with constant stirring. The excess H₂S was trapped in the NaOH solution. The amount of hydrogen evolved was measured using a graduated gas burette. The experimental setup for measuring hydrogen production from H₂S under sunlight is shown in ESI II.†

2.5. Photocatalytic study of splitting of H₂O

To evaluate the photocatalytic activity for the generation of hydrogen from the splitting of water, a xenon lamp ($\lambda \geq 430$ nm) was used as the source of visible light. The photocatalyst was suspended in a quartz photochemical reactor with a water-cooled quartz immersion well and a water jacket with a thermostat. A high-pressure xenon lamp source (300 W) with a cutoff filter was used. The reactor containing the catalyst with the sacrificial agents Na₂S and Na₂SO₃ was vigorously stirred at a constant temperature and purged with Ar for 30 min. Each experiment was carried out using 0.5 g of catalyst in 100 mL of solution. The amount of hydrogen evolved was determined by gas chromatography (Nucon Model 5765, India).

3. Results and discussion

Fig. 1 shows the XRD pattern of the Bi₂S₃ samples synthesized in: water medium, 24 h (S1); water-EG (1 : 3), 24 h (S2); and water-EG (1 : 3), 30 h (S3). All the diffraction peaks match the standard JCPDS data (no. 060333). All the planes were indexed, indicating a pure orthorhombic phase of Bi₂S₃, and they were all equally crystalline.

The optical properties of the samples were investigated by UV-visible diffused reflectance spectrometry (DRS). Fig. 2 shows the UV-DRS spectrum of Bi₂S₃ synthesized by the solvothermal method using different solvents. The direct band gap of the S1, S2 and S3 samples of Bi₂S₃ was observed to be at 1.42, 1.48 and 1.45 eV, respectively which is higher than the bulk sample (1.3 eV).¹¹⁻¹³ The blue shift in the band gap energy was observed as a result of the nanocrystalline nature of the samples.

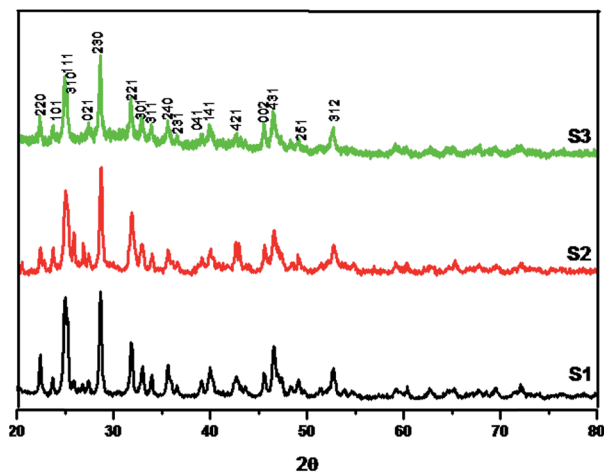


Fig. 1 XRD results for Bi_2S_3 synthesized by the solvothermal method at 150°C with different solvents: (S1) water, 24 h; (S2) water–EG (1 : 3), 24 h; and (S3) water–EG (1 : 3) 30 h.

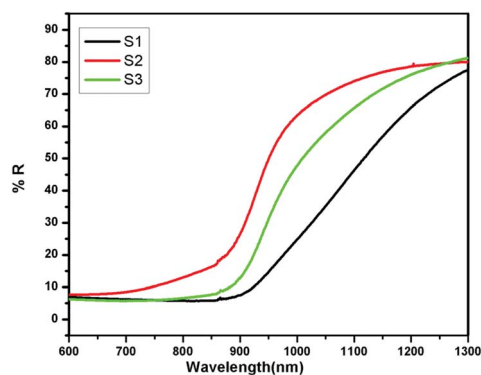


Fig. 2 UV-visible spectra of Bi_2S_3 samples S1, S2 and S3 synthesized by the solvothermal method at 150°C .

Fig. 3a and b show the FESEM images of Bi_2S_3 prepared at 150°C for 24 h (S1) in water. These images show nanorods 30–50 nm in diameter and 2–4 μm in length. The nanorods are random in size and are not aligned. The growth of Bi_2S_3 is very fast in water and therefore randomly distributed, and unevenly sized nanorods are formed.

When the reaction was carried out for 24 h in water–EG (1 : 3), hierarchical nanostructured dandelion flowers (Fig. 3c and d) 1–2 μm in size were observed. The nanorods of diameter 20–50 nm self-aligned and were oriented to form a flower-like morphology: all the nanorods grew radially out from the centre. When the reaction time was increased to 30 h, hierarchically nanostructured flowers (Fig. 3e and f) of size 2–4 μm were formed by the self-alignment of nanorods of diameter 100–150 nm. The flowers were well defined and were formed by the self-alignment of well separated nanorods, which were puffy as compared with the sample S2. Larger flowers with nanorods of a larger diameter were obtained because crystal growth was favoured as a result of the prolonged reaction time *via* the Ostwald ripening phenomenon.²⁵

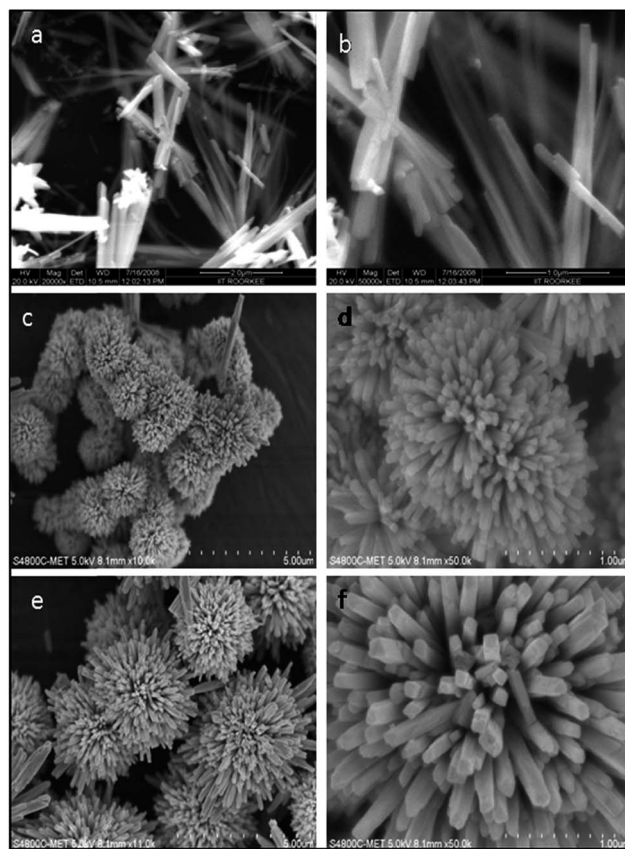


Fig. 3 FESEM images of the Bi_2S_3 samples synthesized by the solvothermal method at 150°C : (a and b) sample S1; (c and d) sample S2; and (e and f) sample S3.

TEM studies (Fig. 4) revealed the morphological variations in the hierarchical Bi_2S_3 samples obtained by the solvothermal method. Fig. 4a shows Bi_2S_3 rods with a size range of 30–50 nm, which was confirmed by FESEM analysis. The corresponding electron diffraction (ED) pattern shows good crystallinity and the d values calculated match the results from XRD. TEM images of samples S2 (Fig. 4c) and S3† (Fig. 4e) show the flower-like morphology seen in the FESEM images. The TEM images show rods with diameters consistent with those of the FESEM images. The corresponding ED pattern shows an orthorhombic structure in agreement with the calculated d values. The bright spots in the ED pattern show the single-crystalline nature of the material.

Photoluminescence (PL) measurements of Bi_2S_3 were made at room temperature at an excitation wavelength of 450 nm (Fig. 5). The spectrum consists of one strong emission peak at 510 nm that can be ascribed to a high-level transition in the Bi_2S_3 semiconductor nanocrystallites. All the products have a peak around 510 nm. However, the peak intensity for the urchin-like flower morphology is less than that for the nanorods.²⁷ This is a result of the surface defects or surface states created by the morphology and the smaller particle size.^{28,29}

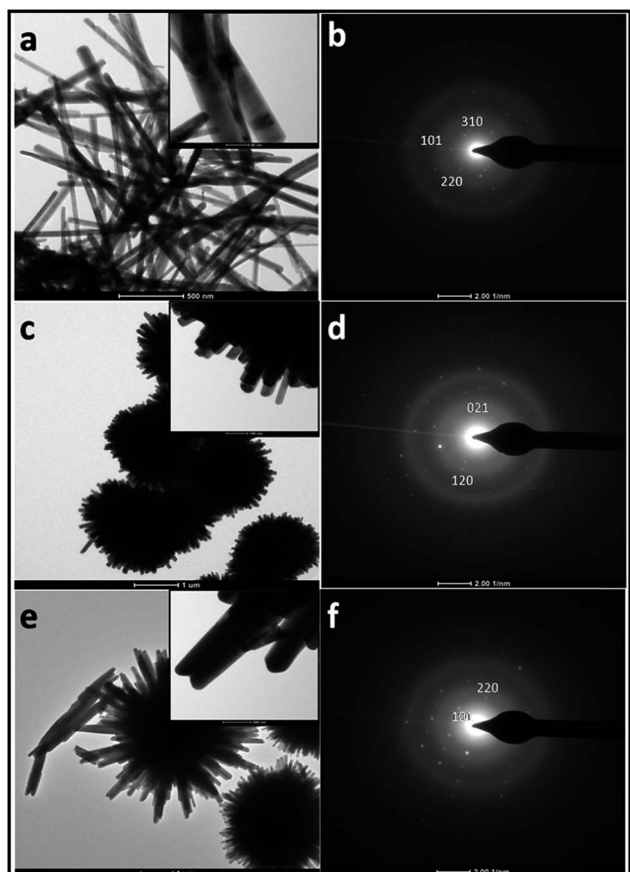


Fig. 4 TEM images of the Bi_2S_3 synthesized by the solvothermal method at $150\text{ }^\circ\text{C}$: (a and b) sample S1; (c and d) sample S2; and (e and f) sample S3.

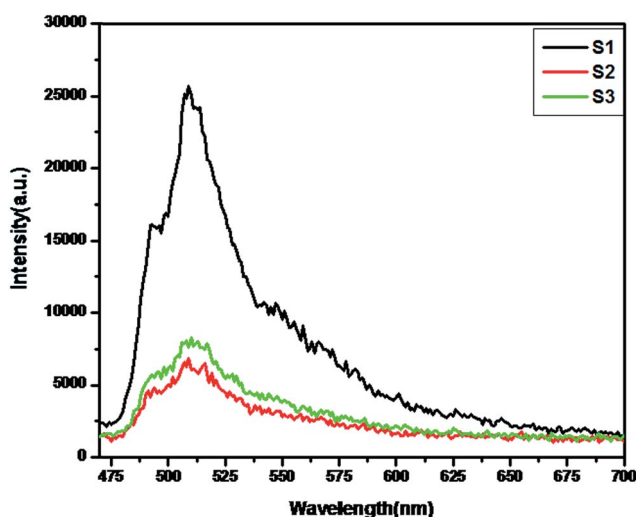
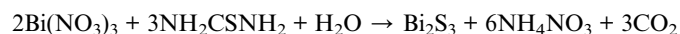
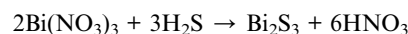
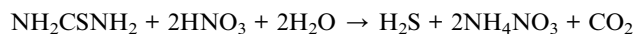
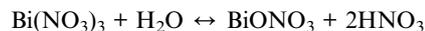


Fig. 5 Photoluminescence spectra of the Bi_2S_3 samples S1, S2 and S3.

4. Mechanism

The hydrothermal method provides a uniform heating environment under pressure, which results in more simultaneous

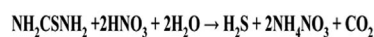
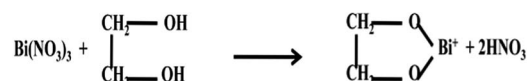
nucleation than conventional methods. The solvents have an influence on the morphologies of the products and favour the synthesis of Bi_2S_3 with different pathways. The formation reaction may be described as follows:²⁶



The growth of the Bi_2S_3 nanorods accelerates *via* nucleation and crystal growth mechanism. $\text{Bi}(\text{NO}_3)_3$ hydrolyses strongly in water and reacts with the TU. The strong attraction between Bi^{3+} and TU leads to the formation of Bi-TU complexes.^{26,30} At the same time, HNO_3 reacts with TU and formation of H_2S , ammonium nitrate and carbon dioxide takes place. The rate of formation of H_2S is very slow before the solvothermal process, but at high temperatures and pressures the rate of formation of H_2S is increased.³¹

The Bi_2S_3 nuclei are formed by the reaction of the Bi^{3+} ions present in the solution with H_2S under hydrothermal conditions. Further growth of the Bi_2S_3 nuclei takes place as the reaction time is increased. Bi_2S_3 is a lamellar structure with Bi_2S_3 units linked to form infinite chains parallel to the *c*-axis. The stronger covalent bond between the planes perpendicular to the *c*-axis facilitates a higher growth rate along the *c*-axis. The much weaker Van der Waals bonding between the planes perpendicular to the *a*-axis limits the growth of the nanorods in the horizontal direction and facilitates their cleavage to form a one-dimensional nanostructure.³¹

In this reaction, when EG-water was used as the reaction medium, the EG acted as a coordination agent. Bismuth nitrate and TU were dissolved in the mixed solvent (EG and water) with magnetic stirring. No precipitation was observed when the two solutions were mixed together and the solution was yellowish and transparent under stirring, unlike the water-only system. This might be attributed to the coordination of EG.^{32,33} The use of EG results in the formation of a complex of bismuth with hydroxide *via* coordination. As a result of the higher temperature and pressure in the solvothermal process, the complex gradually decomposes to release bismuth ions. The Bi_2S_3 nuclei are formed by the reaction of the Bi^{3+} ions present in the solution and the H_2S under solvothermal conditions.



Both TU and EG play important parts in the formation of the hierarchical nanostructures, *i.e.* the flower-like structures. The TU complexes favour oriented growth of the nanorods and also

act as ligands in the formation of the flowers.²⁶ In addition, the powder synthesized in water and the mixed solvent (water-EG) favoured the formation of nanorods and hierarchical flowers, respectively. The high viscosity modified the mobility of the particles in suspension as well as the rates of collision. The EG in the solution results in high adsorption on the inorganic substances, which induces steric hindrance.³⁴ This chemical event probably leads to the minimization of the growth process, causing a reduction in particle size. The interface energy, with a high surface tension between Bi₂S₃ and the mixed solvent, is higher than that in water alone. This interface energy and high surface tension^{35,36} also promote the formation of the self-aligned and organized flower-like morphology. Hence, the formation of nanorods by the water-mediated reaction and the formation of hierarchical nanostructures, *i.e.* flowers, by the reaction mediated by water-EG (1 : 3) is well understood.

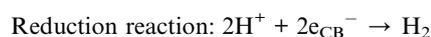
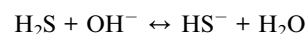
5. Photo-response

The photo-response of the Bi₂S₃ nanorods (sample S1) and the Bi₂S₃ micro-flowers (samples S2 and S3) was measured as a function of time using a white-light source (Fig. 6). The current increased by 1.06 times for S1 (nanorods) and 1.44 and 1.65 times for S2 and S3 (micro-flowers), respectively on exposure to white light (Fig. 6a–c). After switching off the lamp, the current instantaneously decreased to the original value. The on/off cycles could be repeated many times without any detectable degradation in current indicating that all the three Bi₂S₃ samples can be reversibly switched between low and high conductivity. The *I*-*V* curves measured in a large bias range for

the micro-flowers under light and dark conditions are shown in Fig. 6e–f. The slope of the *I*-*V* curves increased when the light was on, indicating enhanced conductivity. However, the micro-flowers (sample S3) showed an increase in slope compared with sample S2. For the nanorods, there was also a slight increase in the slope of the *I*-*V* curve after switching on the light; however, the increase in the slope of the *I*-*V* curve was not significant compared with the two micro-flower samples (Fig. 6d). In these instances, the energy from the light excited the electrons in the semiconductor Bi₂S₃ from the valence band into the conduction band, increasing the charge carrier concentration *via* direct electron-hole pair creation and therefore enhancing the conductivity of the materials.³⁷ It is clear that the conductivity of the Bi₂S₃ micro-flowers is more sensitive to white-light exposure than that of the nanorods. It is believed that multiple internal reflections of light within the interior voids of the micro-flowers are responsible for the enhanced photo-responsive sensitivity of the micro-flower structure compared with the nanorods.³⁸ In particular, the micro-flowers (sample S3) show a slight enhancement in the photo-response compared with sample S2, possibly due to changes in the nature of the flowers. These results suggest that the prepared hierarchical Bi₂S₃ micro-structures are good candidates for applications in high-sensitivity photo-detectors and photo-electronic switches.

6. Photocatalytic activity and measurements

Bi₂S₃ is a semiconductor with a band gap of 1.3–1.7 eV. As a result of its good spectral response to solar light, the photocatalytic activities of Bi₂S₃ have been investigated. We have reported here the extremely high evolution of hydrogen from H₂S splitting under solar light irradiation, in particular for the hierarchical nanostructured Bi₂S₃ flowers compared with Bi₂S₃ nanorods (Table 1). The photocatalytic activities of the as-synthesized Bi₂S₃ without further treatment were evaluated under direct sunlight. In 0.5 M KOH solution, the weak diprotic acid H₂S dissociates and maintains an equilibrium with the hydrogen disulfide (HS⁻) ions. The sulfide semiconductor absorbs light and generates electron-hole pairs. The valence band hole (h_{VB}⁺) photogenerated after the band gap excitation of the Bi₂S₃ powder oxidizes the HS⁻ ion to the disulfide ion (S₂²⁻), liberating a proton from the HS⁻ ion. The conduction band electron (e_{CB}⁻) from the Bi₂S₃ photocatalyst reduces the protons to produce molecular hydrogen.¹⁰ Thus:



The photocatalytic reaction for the evolution of hydrogen was performed using the as-synthesized Bi₂S₃ nanostructures

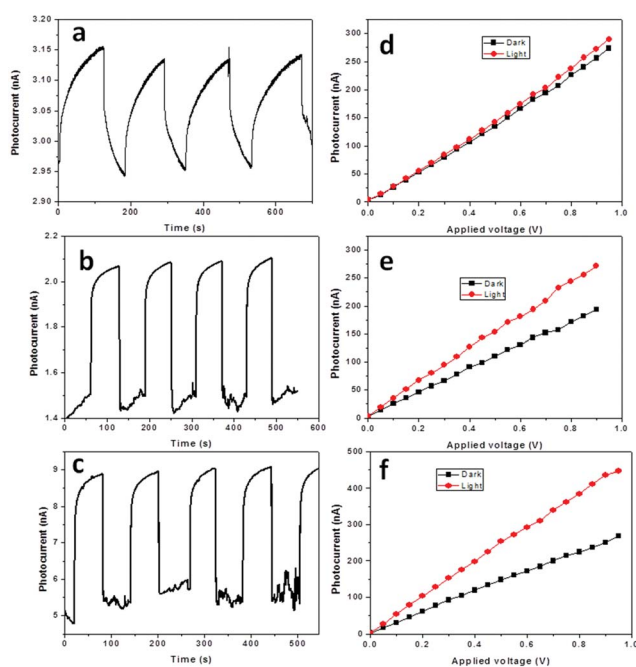


Fig. 6 (a)–(c) Photo-response with time at a bias of 50 mV. (d)–(f) *I*-*V* curves of (d) Bi₂S₃ nanorods (S1), (e) S2 micro-flowers and (f) S3 micro-flowers.

Table 1 BET surface area of synthesized Bi_2S_3 and relation of the rate of hydrogen evolution with different solvents

Sample	S1	S2	S3
BET surface area ($\text{m}^2 \text{g}^{-1}$)	3.71	9.82	6.63
H_2 via H_2S splitting ($\text{mmol g}^{-1} \text{h}^{-1}$)	7.08	8.64	8.88
H_2 via H_2O splitting ($\text{mmol g}^{-1} \text{h}^{-1}$)	0.012	0.017	0.019

under ambient conditions. Different series of experiments were performed to compare the rate of hydrogen evolution by Bi_2S_3 synthesized using different solvents and these results, together with the BET surface area, are summarized in Table 1 and Fig. 7. The maximum hydrogen evolution ($8.88 \text{ mmol g}^{-1} \text{h}^{-1}$) obtained using hierarchical nanostructured Bi_2S_3 (sample S3) was higher (20%) than that of the Bi_2S_3 (S1) nanorods ($7.08 \text{ mmol g}^{-1} \text{h}^{-1}$). However, sample S2 resulted in slightly less (2%) hydrogen evolution compared with sample S3. Both are hierarchical flower-like structures and have good hydrogen evolution, but because of its puffy nature sample S3 has a slightly higher rate of hydrogen evolution.

The PL study clearly showed the lower intensity broad peaks due to surface defects and states created by the hierarchical structure, which ultimately suppress the charge carrier recombination, resulting in the higher photocatalytic activity.

The rate of hydrogen evolution *via* H_2S splitting using sample S3 is better than that of the other samples. A comparative study of H_2 generation using the Bi_2S_3 nanostructures and other reported metal sulfide nanocatalysts was also carried out and the results are given in ESI III.† Although ZnIn_2S_4 has good photocatalytic properties, it is very expensive and the hydrogen evolution requires a xenon lamp; we used natural sunlight in the present study. All the other catalysts investigated were cadmium-based (*i.e.* toxic) and also required a xenon lamp for hydrogen evolution. However, these other photocatalysts also show lower activity than our Bi_2S_3 nanostructures. If we look at the FESEM and TEM images of sample S1 carefully, we can see that rods of different sizes have agglomerated, which ultimately

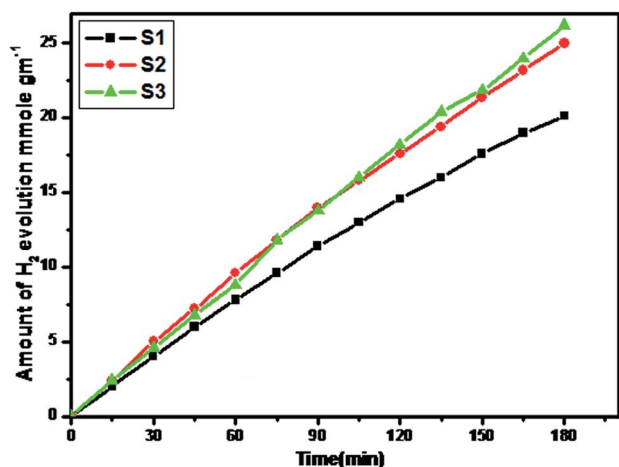


Fig. 7 Hydrogen evolution using Bi_2S_3 samples S1, S2 and S3 obtained *via* H_2S splitting.

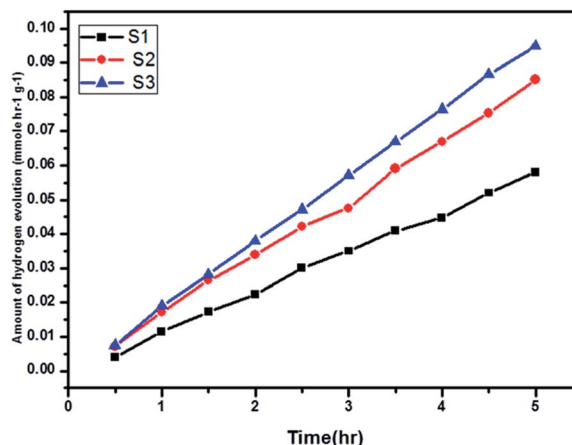


Fig. 8 Hydrogen evolution using Bi_2S_3 samples S1, S2 and S3 obtained *via* H_2O splitting.

reduces the number of effective surface sites available for photoreactions. This is responsible for the slightly lower hydrogen evolution seen with sample S1.

Fig. 8 shows a typical time course of hydrogen evolution from water splitting using samples S1, S2 and S3 under visible light. Hydrogen evolution was not observed without light irradiation (kept for 2 h). However, with irradiation by light, hydrogen was steadily evolved with time. The maximum evolution of hydrogen ($0.019 \text{ mmol g}^{-1} \text{h}^{-1}$) was obtained using the hierarchical nanostructured Bi_2S_3 (sample S3), which had a higher evolution of hydrogen than samples S1 and S2 (0.012 and $0.017 \text{ mmol g}^{-1} \text{h}^{-1}$, respectively). As the reaction was carried out in the presence of the sacrificial agents Na_2S and Na_2SO_3 , an electron donor and the oxygen were not evolved. GC analysis showed the absence of O_2 and N_2 from air.

Fig. 7 and 8 show the time-dependent evolution of hydrogen using the as-synthesized nanostructured Bi_2S_3 . The linearity of the graph clearly shows the stable rate of evolution of the nanostructured Bi_2S_3 . The GC results for the hydrogen gas evolved during the reaction is given in ESI IV.†

The hierarchical nanostructured flowers are self-oriented where the number of effective surface sites has been increased due to their puffiness, which also suppresses the recombination of charge carriers at the surface. In a solid, the charge carriers repeatedly scatter off defects and therefore do not accelerate faster, instead moving with a finite average velocity, called the “drift velocity”. This net carrier motion is usually much slower than the normally occurring random motion and hence the rate of recombination is slower; this effectively results in the enhanced photocatalytic activity of the material. Electron transport to the surface may increase due to the puffiness and hence more hydrogen is evolved from sample S3. The slight increase in the rate of hydrogen evolution from sample S2 may be due to the compact hierarchical flower-like morphology.¹⁰ The PL study showed that the flower-like morphology has more surface defects that enhance the charge carrier separation. This was also confirmed by the photo-response study. This could also be one of the reasons for obtaining a high photocatalytic activity for the Bi_2S_3 flowers.

The stability of the S1, S2 and S3 photocatalysts was examined by reusing the photocatalyst samples (after H₂S splitting). XRD analysis of the reused catalysts (RS1, RS2 and RS3) did not show a change in the phase purity of Bi₂S₃ (ESI V†). The evolution of hydrogen from the reused catalysts is also given in ESI VI.† The rate of hydrogen evolution by H₂O splitting is low compared with that from H₂S splitting. Bi₂S₃ is a good photocatalyst for the production of hydrogen from H₂S.

7. Conclusions

We have demonstrated the fabrication of single-crystalline nanorods and hierarchical nanostructures by a simple one-pot solvothermal method. The water-mediated reaction produces nanorods and the reaction mediated by the mixed solvent (water-EG) confers hierarchical nanostructures (flowers) of Bi₂S₃. The high interface energy and surface tension are responsible for this flower-like morphology. The as-prepared Bi₂S₃ photocatalyst showed a high photocatalytic activity for the evolution of hydrogen by H₂S splitting under normal sunlight. Excellent photocatalytic activity for hydrogen production *via* H₂S splitting under normal sunlight was also obtained. It is noteworthy that the hierarchical nanostructured Bi₂S₃ (dandelion flowers) show a significant rate of evolution of hydrogen without any promoters. The evolution of hydrogen from water splitting was also observed for all samples; the flower-like Bi₂S₃ showed a higher rate of evolution of hydrogen than the other structures.

Acknowledgements

The authors thank the Department of Electronics and Information Technology (DeitY), New Delhi for financial support. We also thank the Executive Director, C-MET, Pune and Nano-crystalline Material Group, C-MET, for supporting this work.

References

- 1 A. Fujishima and K. Honda, *Nature*, 1972, **238**, 37.
- 2 J. Sun, G. Chen, G. Xiong and H. Pei Dong, *Int. J. Hydrogen Energy*, 2013, **38**, 10731.
- 3 Q. Xiang, J. Yu and M. Jaroniec, *J. Am. Chem. Soc.*, 2012, **134**, 6575.
- 4 (a) K. M. Parida, S. Pany and B. Naik, *International Journal of Hydrogen Energy*, 2013, **38**, 3545; (b) C. Li, W. Chen, J. Yuan, M. Chen and W. Shangguan, *World J. Nano Sci. Eng.*, 2011, **1**, 79.
- 5 S. Apte, S. Garaje, G. Mane, A. Vinu, S. Naik, D. Ambalnerkar and B. Kale, *Small*, 2011, **7**, 957.
- 6 A. Bhirud, N. Chaudhari, L. Nikam, R. Sonawane, K. Patil, J. Baeg and B. Kale, *Int. J. Hydrogen Energy*, 2011, **36**, 11628.
- 7 A. Bhirud, D. S. Sathaye, R. Waichal, L. Nikam and B. Kale, *Green Chem.*, 2012, **14**, 2790.
- 8 S. Garaje, S. Apte, S. Naik, J. Ambekar, R. Sonawane, M. Kulkarni, A. Vinu and B. Kale, *Environ. Sci. Technol.*, 2013, **47**, 6664.
- 9 S. Apte, S. Garaje, M. Valant and B. Kale, *Green Chem.*, 2012, **14**, 1455.
- 10 (a) N. Chaudhari, A. Bhirud, R. Sonawane, L. Nikam, S. Warule, V. Rane and B. Kale, *Green Chem.*, 2011, **13**, 2500; (b) B. B. Kale, J. O. Baeg, K. Kong, S. Moon, L. K. Nikam and K. R. Patil, *J. Mater. Chem.*, 2011, **21**, 2624; (c) S. K. Apte, S. N. Garaje, S. S. Arbu, B. B. Kale, J. O. Baeg, U. P. Mulik, S. D. Naik, D. P. Amalnerkar and S. W. Gosavi, *J. Mater. Chem.*, 2011, **21**, 19241; (d) S. N. Garaje, S. K. Apte, S. D. Naik, J. D. Ambekar, R. S. Sonawane, M. V. Kulkarni, A. Vinu and B. B. Kale, *Environ. Sci. Technol.*, 2013, **47**, 6664; (e) B. B. Kale, J. O. Baeg, S. M. Lee, H. Chang, S.-J. Moon and C. W. Lee, *Adv. Funct. Mater.*, 2006, **16**, 1349.
- 11 C. Song, D. Wang, T. Yang and Z. Hu, *CrystEngComm*, 2011, **13**, 3087.
- 12 G. Konstantatos, L. Levina, J. Tang and E. Sargent, *Nano Lett.*, 2008, **8**, 4002.
- 13 L. Li, N. Sun, Y. Huang, Y. Qin, N. Zhao, J. Gao, M. Li, H. Zhou and L. Qi, *Adv. Funct. Mater.*, 2008, **18**, 1194.
- 14 Z. Liu, W. Huang, Y. Zhang and Y. Tong, *CrystEngComm*, 2012, **14**, 8261.
- 15 C. Li, W. Chen, J. Yuan, M. Chen and W. Shangguan, *World J. Nano Sci. Eng.*, 2011, **1**, 79.
- 16 R. Brahimi, Y. Bessekhoud, A. Bouguelia and M. Trari, *Catal. Today*, 2007, **122**, 62.
- 17 F. Liu, Y. Yang, J. Liu, W. Huang and Z. Li, *J. Electroanal. Chem.*, 2012, **665**, 58.
- 18 J. Kim and M. Kang, *Int. J. Hydrogen Energy*, 2012, **37**, 8249.
- 19 Y. Bessekhoud, M. Mohammedi and M. Trari, *Sol. Energy Mater. Sol. Cells*, 2002, **73**, 339.
- 20 A. Tahir, M. Ehsan, M. Mazhar, K. Upul, W. Zeller and A. D. Hunter, *Chem. Mater.*, 2010, **22**, 5084.
- 21 L. Cademartiri, F. Scotognella, P. O'Brien, B. Lotsch, J. Thomson, S. Petrov, N. Kherani and G. Ozin, *Nano Lett.*, 2009, **9**, 1482.
- 22 Y. Yu and W. Sun, *Mater. Lett.*, 2009, **63**, 1917.
- 23 L. Dong, Y. Chu and W. Zhang, *Mater. Lett.*, 2008, **62**, 4269.
- 24 X. Zhou, H. Shi, B. Zhang, X. Fu and K. Jiao, *Mater. Lett.*, 2008, **62**, 3201.
- 25 M. Ibanez, P. Guardia, A. Shavel, D. Cadavid, J. Arbiol, J. Morante and A. Cabot, *J. Phys. Chem. C*, 2011, **115**, 7947.
- 26 C. Tang, C. Wang, F. Su, C. Zang, Y. Yang, Z. Zong and Y. Zhang, *Solid State Sci.*, 2010, **12**, 1352.
- 27 Y. Xu, Z. Ren, G. Cao, W. Ren, K. Deng and Y. Zhong, *Physica B*, 2010, **405**, 1353.
- 28 X. Zhu, J. Ma, Y. Wang, J. Tao, B. Lin, Y. Ren, X. Jiang and J. Liu, *Ceram. Int.*, 2008, **34**, 249.
- 29 C. Tang, J. Su, Q. Hu, Y. Yang, C. Wang, C. Zhao, C. Zang and Y. Zhang, *Solid State Sci.*, 2011, **13**, 1152.
- 30 T. Thongtem, A. Phuruangrat, S. Wannapop and S. Thongtem, *Mater. Lett.*, 2010, **64**, 122.
- 31 M. Niasari, D. Ghanbaria and F. Davara, *J. Alloys Compd.*, 2009, **488**, 442.
- 32 G. Tian, Y. Chen, W. Zhou, K. Pan, Y. Dong, C. Tian and H. Fu, *J. Mater. Chem.*, 2011, **21**, 887.

- 33 M. Shang, W. Wang and H. Xu, *Cryst. Growth Des.*, 2009, **9**, 991.
- 34 V. S. Marques, L. S. Cavalcante, F. P. Alcantara, M. O. Orlandi, E. Moraes, J. A. LongoVarela, M. S. Li and M. R. M. C. Santos, *Cryst. Growth Des.*, 2010, **10**, 4752.
- 35 G. Zhu, P. Liu, J. Zhou, X. Bian, X. Wang, J. Li and B. Chen, *Mater. Lett.*, 2008, **62**, 2335.
- 36 V. S. Marques, L. S. Cavalcante, J. C. Sczancoski, A. F. P. Alcantara, M. O. Orlandi, E. Moraes, E. Longo, J. A. Varela, M. SiuLi and M. R. M. C. Santos, *Cryst. Growth Des.*, 2010, **10**, 4752.
- 37 H. F. Bao, X. Q. Cui, C. M. Li, Y. Gan, J. Zhang and J. Guo, *J. Phys. Chem. C*, 2007, **111**, 12279.
- 38 L. Lianshan, R. Cao, Z. Wang, J. Li and L. Qi, *J. Phys. Chem. C*, 2009, **113**, 18075.